1 Introduction

The extent to which soil strength is altered by earthquake loading is an issue of key importance in geotechnical engineering. It is a well known behaviour that in the presence of cyclic loading, the resistance of loose sands to resist vertical loads is diminished. This is the cause of billions of dollars worth of damage every year and substantial soil failures. As always in the field, the initial ground conditions play a key role in determining the response of the foundations.

Liquefaction

A phenomenon which has a large effect on the strength of soil is the process of liquefaction. This occurs when saturated fine sands or silts succumb to a large reduction in strength during cyclic loading. This occurs due to the lack of effective stress between soil particles, as a result of increasing pressure of the pore fluid. Loose sand tends to contract into a more efficient packing under cyclic loading leading to settlement. However, the porosity of the sand does not permit pore fluid movement in response to this tendency, and therefore is resisted by an increase in pore pressure. Terzaghi's Principle states that stresses are carried by both soil grains (effective stress) and pore pressures:

$$\sigma' = \sigma - u$$

It is also known that cohesionless, frictional, soils shear resistance is generated from friction, which is in turn proportional to the effective stress. It follows that an increase in pore pressure will result in the reduction of strength of a Mohr Coulomb soil.

As a result, large increases in pore pressures which can occur during earthquakes can lead to greatly reduced strengths of sand, sometimes resulting in complete soil failure.

Fig. 1.1 - Foundation failure following liquefaction

This phenomenon came to prevalence in the aftermath of the 1964 Niigata earthquake, where much of the city's infrastructure was destroyed, however major liquefaction events have occurred since, including in Izmit, Turkey (1999, figure 1.1), and

Fig. 1.2 - Differential Structural Settlements following Liquefaction

more recently, during the Christchurch earthquake in 2012. Damage to buildings and services during liquefaction events is severe, as buoyancy effects cause severe differential settlements (figure 1.2).

Much work has been carried out in order to quantify the reduction in bearing capacity during earthquake movements in dry sand. Limiting equilibrium and kinematic solutions have been proposed in closed form and numerical/empirical studies undertaken to account for phenomena such as uplift (mech 2, Paolucci & Pecker, (1997)) and peak moments acting along the base,

Project Aims

This project aims to expand the investigation into the behaviour and form of failure for loose, saturated sandy soils under earthquake loading. Having established a link between theoretical bearing capacities and actual soil movements in a test environment for dry soils (Knappett, 2006), it is hoped that the reverse can be applied in the case of liquefiable soils. By observing failures experimentally, attempts can be made to generate kinematic and limiting equilibrium solutions to the reduction of strength of a soil as it undergoes liquefaction

2 Review of Literature

2.1 Development of Analytical Solutions for Shallow foundation Failure Mechanisms

Prandtl solution (1956)

Prandtl developed his solution to bearing capacity of a semi infinite strip footing on undrained soil by considering both kinematic and equilibrium solutions for failure mechanisms. For the undrained solution, critical state soil mechanics relates fixed density shear stress at failure. This allows a solution to be generated without the need to determine the effective stress. In defining mechanisms which satisfy equilibrium, a series of lower bound solutions can be calculated. Similarly, defining kinematic mechanisms which describe energy dissipation yields an upper bound solution to the bearing capacity. The Prandtl mechanism is one which satisfies both simultaneously, giving the same capacity for both limiting equilibrium and kinematic considerations (equation 1)

$$\frac{V}{A} = q = Nc(2 + \pi)su$$

The same methodology has been applied to drained capacity of strip footings on drained soils. In the drained case, strength is governed by the frictional capacity of the soil, which in turn is dependent on the in situ effective stresses in the soil.

Paolucci & Pecker (1997): Mech2 shallow foundation failure mechanism

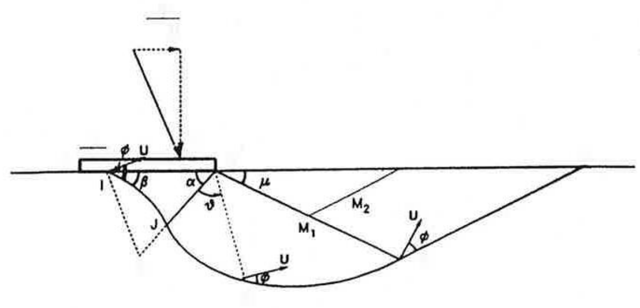

Work carried out by Paolucci and Pecker (1997) extended the idea of producing solutions for failure mechanisms, in order to understand soil behaviour under seismic loading. The analysis has produced a mechanism which includes parameters to allow for uplift of the foundation due to seismic loading, which is a common feature of shallow foundations in dry soils, where rocking can occur.

PIV Verification – Knappett (2003)

Knappett (2003) conducted 1g shaking experiments on dry soil, capturing footage of the soil mechanism using a high frame rate camera. The resulting Particle Imaging Velocimetry analysis was compared against bearing capacity mechanisms for dynamic loading of soils. The analysis confirmed the mech2 mechanism proposed by Paolucci and Pecker (Figures X and Y).

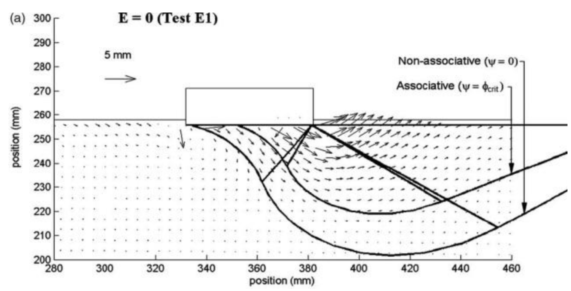

3 Experimental Procedure

3.1 Apparatus & Instrumentation

3.1.1 1g Shaking Table

The experiments will take place on the 1g shaking table at the Schofield Centre. This consists of a computer controlled motor which drives a flywheel, coupled to a driveshaft with an offset mass, delivering a specified amplitude and frequency to the shaking table. The shaking table is capable of delivering up to 10 seconds of vibration with amplitude of up to 5mm and frequency up to 5Hz, which corresponds to a peak ground acceleration of 0.5g. The table consists of a watertight sandbox with three steel sides and a Perspex viewing panel with dimensions of 0.7m x 0.3m x 0.5m (see figure 3.1).

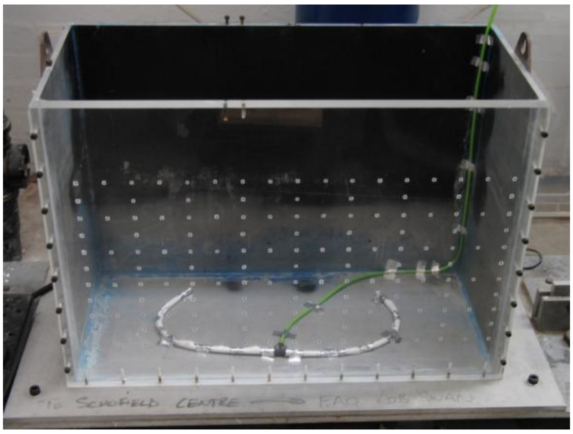

Figure 3.1 - Shaking table rig

3.1.2 Soil Model

The soil model consists of saturated Hoston sand to a depth of 25cm. The Hoston sand is a silica sand, with a specific gravity of 2.65, emax of 1.067, emin of 0.555 and has a critical friction angle $\varphi=30^{o}$. Instrumentation to measure the acceleration and pore pressure response of the soil model will be inserted in the model at various elevations, depending on the specific test being undertaken (Section X).

3.1.3 Motion Blitz High Speed Camera

Images of the foundation failures will be obtained using the Motion Blitz High Speed Camera. The camera is capable of capturing up to 1000 frames per second, at a resolution of 3 megapixels. The camera is attached directly to a computer via a network cable, and the images are processed with MotionBlitz9.0 software. The images will be analysed using Particle Image Velocimetry in order to obtain movements of the soil under the footing during and after earthquake motions. The high frame rate capability of the camera is essential to capture the motion of the footings, particularly given that large total deformations are expected. This will ensure that images are sufficiently similar such that the PIV software can track soil particles and movements accurately.

3.1.4 Microelectromechanical (MEM) Accelerometers

MEM's have been placed in the soil model to measure the vertical and horizontal accelerations experienced by the soil. This will allow the relationship between the amplitude and phase of the soil accelerations with that of the shaking table to be investigated. Where possible the MEM's have been rated at 1.7g, i.e. the maximum accelerations which can be measured. This is comparable with the maximum anticipated accelerations of approximately 0.5g. This will allow sufficient resolution for the equipment to measure the accelerations. It must be noted that, as opposed to piezo accelerometers, MEM accelerometers measure static forces due to gravity, and are directionally sensitive, thus providing a constant output, even when not undergoing any accelerations.

3.1.5 Pore Pressure Transducers (PPTs)

The transducers measure the pressure of the pore fluid at a given instant. It is expected that readings from the PPTs will give an indication as to the extent of liquefaction in the soil during the tests. In addition, the effective stress in the soil can be calculated, allowing further comparison with the accelerations of the soil. The PPTs being used have a range of 35kPa, which is appropriate for the predicted confining pressures. These instruments require careful calibration, which is undertaken at the centre in the deaired calibration rig.

3.1.6 Linear Variable Differential Transformer LVDT

A linear Variable Differential Transducer allows linear displacement to be measured. This instrument is placed on the edge of the shaking table, allowing the rigid body movement of the box to be measured. Accelerations of the box can be obtained from the displacements with time, allowing comparison with accelerometer data.

3.1.7 Junction Box

Experimental information is connected to a junction box, which amplifies signals before passing them to the datalogger. The junction box is configured given the required inputs. In these experiments, data will be logged with DASYLAB9.0 software, as standard in the Schofield Centre.

3.1.8 Foundation Model

The foundation bearing pressure is applied by way of a brass block (density of 7840kg/m^3), of dimensions (100 x 40 x 295 mm). This allows the high and low aspect ratio models to exert 7.7kPa and 3.07 kPa respectively when the box is placed on its side (fig. 3.2) and on its end. The length of the block is the almost same as that of the 1g shaking table, allowing the model to act as a strip footing. With this in mind it is assumed that the deformations will occur in plane strain, and that there are no edge effects. In order to minimise friction between the block and the perspex front of the shaking table, a PTFE face has been included on the brass block. in addition, there is a small amount of clearance between the block and the back of the shaking table. This is because it has been found that when fully wedged, despite the PTFE coating, free movement of the block is inhibited. As a result, during some of the tests the block came away from the Perspex viewing window, a gap of approximately 2mm being observed. Control markers have been added to this face to enable tracking of the foundation's settlement using the PIV method, discussed in section 4.

fig 3.2 – Foundation Model

3.2 Model Preparation

3.2.1 Sand pouring

The soil model of loose sand has is poured manually using a hopper in the Schofield Centre. The relative density of the sand model was maintained at 0.35-0.5, such that multiple earthquakes could be conducted with the model. As discussed in Section 2.1, the sand model will tend to contract after liquefaction occurs, making subsequent earthquakes less likely to result in liquefaction. This behaviour governed the earthquake sequence in each test, moving from smaller peak acceleration vibrations to larger ones, to ensure the best chance of a successful earthquake.

The ideal conditions for pouring loose sand have been identified as having a high flow rare and small clearance between the nozzle and sand surface. In order to reduce the likelihood of creating weak strata whilst pouring, layers were poured perpendicular to the previous layer. In order to mitigate the risks associated with exposure to sand dust in the test room, personal safety equipment such as dust extractors and dust masks were utilised (see 'Appendix B, Risk Assessment Retrospective' for further details).

3.2.2 Sand Dying

In order to increase the texture of the sand model, such that the PIV software could better track soil patches (see Section 5.3), pure Hoston sand was blended with Hoston sand dyed blue in a ratio of 10:1 . Blue metallic paint was mixed with Hoston sand manually, before mixing the two proportions in the hopper, ensuring an even distribution. It is not thought that the addition of the paint would affect the material properties of the sand.

In order to aid visualisation of the soil deformation during the testing, concentrated blue sand was added to the model at the elevations of the instrumentation. This was to give an indication of whether or not the instruments were likely to have moved, as well as providing a visual indication of the form of the failure mechanisms.

3.2.3 Saturation with pore fluid

In order to facilitate saturation of the soil model, piping was installed in the base of the 1g shaking table (figure 3.1). This consisted of PVC tubing with filter paper positioned over the holes, in order to reduce the risk of them being blocked by the sand. The model is saturated from the bottom up to allow the expulsion of air, reducing the risk of air pockets forming which could lead to heterogeneity of behaviour, as well as the possibility of disturbing the model during earthquake motions.

An important consideration in saturation is that of de-airing water before using it for saturation fluid. This is due to the tendency of dissolved gasses to come out of solution during testing, resulting in spoiled test results. The water is de-aired in a vacuum chamber, before being added to a head tank situated by the model. The model is then saturated by applying a gravity head. Care is taken to ensure that the pore fluid will not cause liquefaction of the soil, which could occur if an overtly large pressure head was applied.

Methyl Cellulose

Methyl cellulose is a reagent which dissolves in water to increase its viscosity. As the test programme is conducted in 1g conditions, in situ stresses and pore pressures are lower than in reality. This, coupled with the smaller drainage distances due to the size of the footing, has been shown to inhibit excess pore pressure generation as dissipation occurs at a higher rate than would be expected in reality. Adding methyl cellulose to create a more viscous fluid is hoped to allow larger peak excess pore pressures to be created, giving more representative pore pressures in the model. 1g shaking table scaling laws suggest that the permeability of the soil layer should scale with $\lambda^{0.75}$ (after Iai, S. (1989). For a scale factor of 1/100, viscosity should be increased by a factor of 31. However, this is practically infeasible in this case, given that the apparatus is unsuitable for saturation to be supplemented with a vacuum to increase the saturation head.

The design viscosity is 8-10 centistroke (1 centistroke = $1x10^{-6}$ m^2/s), giving the pore fluid a viscosity of approximately 10 times that of water. The amount required follows the equation

$$v_{20} = 6.8C^{2.34}$$

which fits test data for the viscosity profile with concentration of Methylcellulose (Douglas P Stewart et. al – 1998).

The appropriate amount of methylcellulose powder was added to three 10litre buckets of de-aired water, which increased the surface area to allow the powder to dissolve more effectively. The viscosity of each bucket was tested using a viscometer, before the mixture being added to the head tank to allow saturation to take place. Given the greater viscosity of the pore fluid this procedure took much longer than with water as a pore fluid. Problems were encountered during the saturation of test three, where it became apparent that a gravitational head provided by the crane was insufficient to overcome the losses induced in the pipes, stalling saturation. This resulted in additional saturation tubes being placed in the sides of the model, disturbing the sand in the process. The saturation regime was changed for test four, where the filter paper was replaced with a drainage layer consisting of grade A sand covering the saturation tube, and a 2cm layer of grade B sand atop .It was envisaged that such a procedure would reduce the likelihood of sand particles blocking the tube, without it being blocked by methylcellulose either. This approach resulted in a successful saturation procedure.

3.3 Model setup

Test 1 : Low Aspect Ratio- Water pore Fluid

The structural model was placed on top of the saturated soil model at an elevation of 250mm. Horizontal and vertical MEM accelerometers placed along the centre line of the structural model at elevations of 100mm and 200mm, corresponding to the w/2 and 3w/2 respectively. Pore pressure transducers were installed along the centre line of the model at an elevation of 20mm in order to measure the pore pressure response under the footing and 200mm to the side of the model centreline in order to obtain 'free field' pressure conditions.

Test 2: High Aspect Ratio – Water Pore Fluid

The structural model was placed on top of the saturated soil model at an elevation of 250mm. Horizontal and vertical MEM accelerometers placed along the centre line of the structural model at elevations of 170mm and 210mm, corresponding to a depth of w and 2w respectively. One pore pressure transducers was installed along the centre line of the model at an elevation of 210mm in order to measure the pore pressure response under the footing.

Test 3: High Aspect Ratio – Methyl Cellulose Pore Fluid

The structural model was embedded to a depth of 40mm into the saturated soil model whose surface was at an elevation of 250mm. Horizontal and vertical MEM accelerometers placed along the centre line of the structural model at elevations of 140mm and 170mm, corresponding to a depth of w and 2w respectively. One pore pressure transducer was installed along the centre line of the model at an elevation of 170mm in order to measure the pore pressure response under the footing.

Test 4: Low Aspect Ratio – Methyl Cellulose Pore Fluid (Include Figures)

The structural model was embedded to a depth of 40mm into on top of the saturated soil model whose surface was at an elevation of 250mm. Horizontal and vertical MEM accelerometers placed along the centre line of the structural model at elevations of 140mm and 170mm, corresponding to a depth of w and 2w respectively. One pore pressure transducer was installed along the centre line of the model at an elevation of 170mm in order to measure the pore pressure response under the footing.

3.4 Experimental Programme

In order to achieve the aims of the project, an experimental programme consisting of four tests has been proposed. These will investigate the role of structural aspect ratio, and pore fluid viscosity in the behaviour of the soil.

Test Number	**Aspect Ratio**	**Pore Fluid**	**Earthquake 1**		**Earthquake 2**		**Earthquake 3**	
			Amplitude (mm)	**Freq. (Hz)**	**Amplitude (mm)**	**Freq (Hz)**	**Amplitude (mm)**	**Freq (Hz)**
1	Low	Water	2	3.5	2	4	4	4.5
2	High	Water	2	2.5	2	3.5	2	4.5
3	High	Methylcellulose	2	2.5	2	4	2	4
4	Low	Methylcellulose	2	3.5	2	4	4	4.5

The test series will investigate the effect of aspect ratio and pore fluid respectively. Each test involves 3 earthquakes of differing magnitude and frequency. This will allow the soil behaviour to be observed during no liquefaction, partial liquefaction and full liquefaction earthquakes.

Effect of Aspect Ratio

It is anticipated that the two aspect ratios will respond differently in turn. The increased inertial moment on the high aspect ratio structure will lead to rocking effects. The low bearing stress of the low aspect ratio may lead to sliding mechanism being critical. Given the differences in contact areas, the form and depth of the failure mechanisms will differ.

Effect of Pore Fluid

See Section 3.2.3. The addition of a more viscous fluid is known to sustain excess pore pressures for longer. This may lead to different behaviour, such as a longer liquefaction time and higher peak excess pore pressures. The relationship between pore pressure and settlements can be investigated.

3.5 Limitations of model

Scale

Usually in geotechnical modelling, scale models are prepared and tested in a centrifuge, which subjects the model to large accelerations. This allows tests to be carried out at representative stresses, allowing greater correlation of soil behaviours. Given the time constraints related to this project, centrifuge testing was not a feasible option.

Liquefaction events are highly sensitive to confining stresses (as presented by Ishihara, 1993) and the subsequent behaviour is governed by the initial soil conditions. As a result, only qualitative information can be taken from the test series. This information will be used in order to inform further testing in a centrifuge.

Rigid Shaking Table

The rigid sides of the shaking table are likely to reflect pressure waves and stresses due to the accelerations. This will make the data noisy, adding harmonic components. Flexible containers, consisting of layers of slip rings are more effective at minimising reflections, allowing the assumption of a semi infinite half space to be upheld. However, given the need for a transparent window for PIV analysis, these are unsuitable. It is hoped that these high frequency components will be successfully removed during data filtering.

4 Particle Image Velocimetry (PIV)

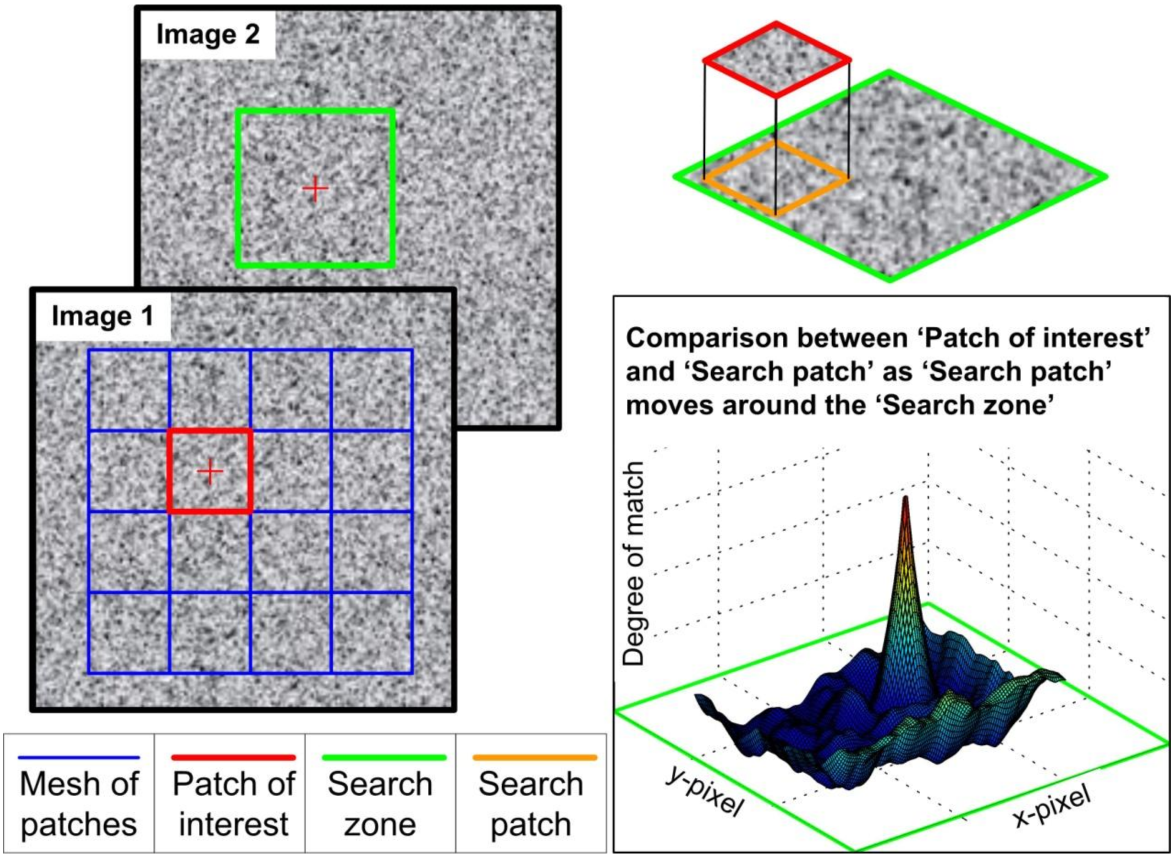

Fig. 4.1**Particle Image Velocimetry**

4.1 Theory

Particle Image Velocimetry is a technique for tracking the movements of particles over the course of an experiment. The experiment is captured by using a high speed camera, capturing up to 1000 frames per second. The soil model is divided into a number of soil 'patches', for which the configuration and intensity of pixels is stored. Software is then utilised which compares frames of the experiment, and searches for the best match from the previous frame, based on a 'search zone' passed by the user. In this way, the movement of each patch is tracked throughout the experiment (fig.4.1). More detailed analysis can allow strains to be calculated in the soil model.

4.1.1Programmes Used

Images from the Fast Camera were stored on computer using the ImageBlitz image capturing software. The PIV analysis is conducted on MATLAB using software created by Cambridge University (after White D.J., & Take W.A (2002). The routine uses launcher files which have the images stored to perform the PIV analysis, calibrations as well as post PIV visualisations (see Results).

4.2 Perspex preparation & PIV Calibration

The experimental programme aims to capture soil movements due to the foundation failure under liquefaction. This requires soil movements relative to that of the shaking table box. This is achieved with the addition of control markers on the face of the Perspex box, consisting of black permanent marker, surrounded by white paint. The white black contrast allows ease of tracking. The control markers also perform the function of converting movements from pixel space to millimetres. The Perspex is polished before the control markers are added, to remove any scratches which may cause serious distortion of light as well as inhibit the free movement of sand particles against the surface.

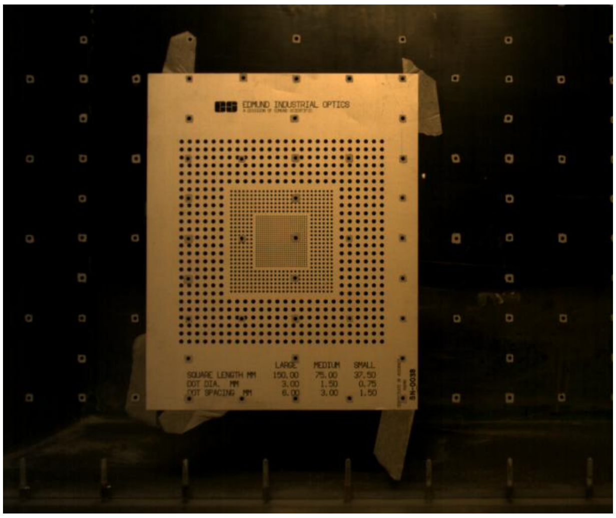

Fig. 4.2 Mylar Card Calibration

Given the images are distorted as they are diffracted through the Perspex, as well as through the lens of the camera, calibration is required to infer the actual position of soil patches from the image. This is achieved with the use of a Mylar Chart, which contains dots of a specified distance apart. Images are taken of the control marker configuration with the Mylar card behind, as in figure 4.3. Given that the relative positions of the dots are known, any distortions arising from imperfections and refraction in the Perspex and the lens in the camera can be accounted for, such that the a position in the camera image corresponds directly to a position in space.

4.3 Input Parameters

Patch Size

The accuracy of the software is sensitive to the patch size selected by the user. This is defined in terms of pixels. Too small a patch and distortions due to the Perspex panel may over ride the texture of the soil deformation, leading to a loss of tracking. Too large and resolution is lost, as well as the influence of the control markers may cause the software to track it instead.

Search Zone

The search zone is defined as the number of pixels from the original 'patch' that the software can search for the closest match. Theoretically the search zone could extend to the full size of the image, however this would lead to an impractically long computing time, and could result in other regions with similar textures (such as other control markers) being tracked instead. The searchzone and leapfrog (below) should be selected together in order to reduce the possibility of wild vectors, where accurate tracking fails.

Leapfrog

The leapfrog parameter specifies the number of frames which are compared with one another. It is important to have as large a leapfrog as possible, as this reduces the accumulated errors which occur during the comparison between images. However, too large a leapfrog can lead to comparisons between images which are too different, and soil patch movements which are greater than the search zone which has been specified.

5 Results

5.1 Earthquake Test Reference Images

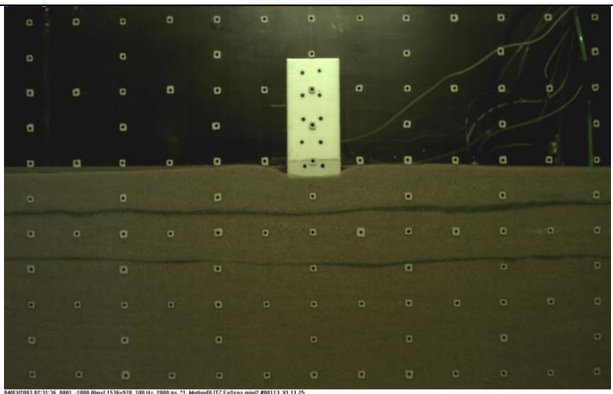	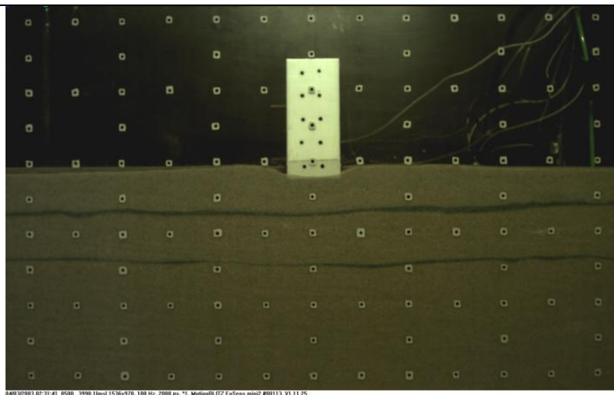
Figure 5.1.1 - Test2 Earthquake 1	2mm Amplitude – 2.5 Hz

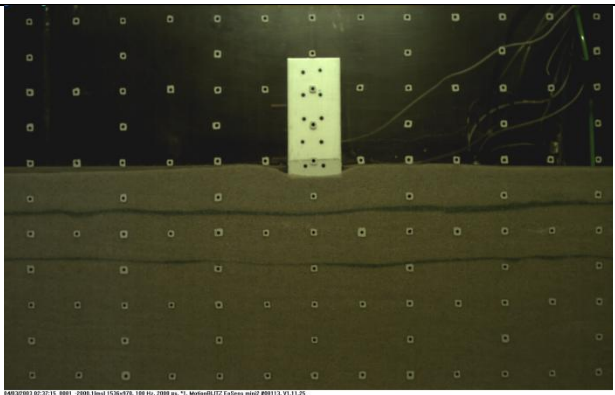	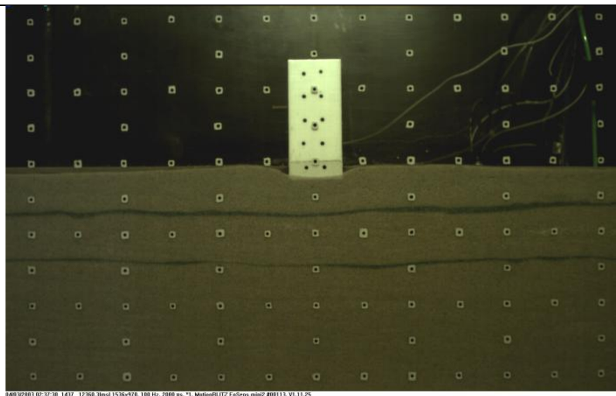
Figure 5.1.2 -Test 2 Earthquake 2	2mm Amplitude – 3.5 Hz

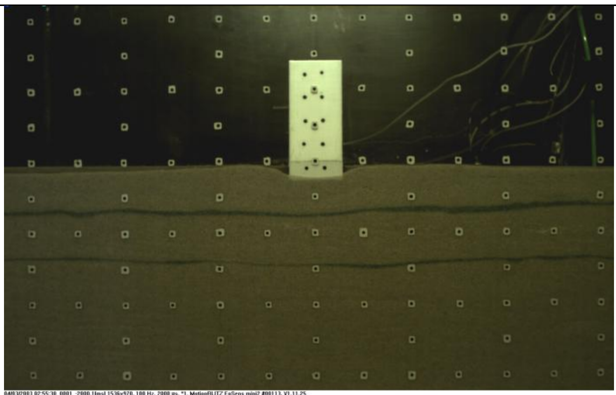	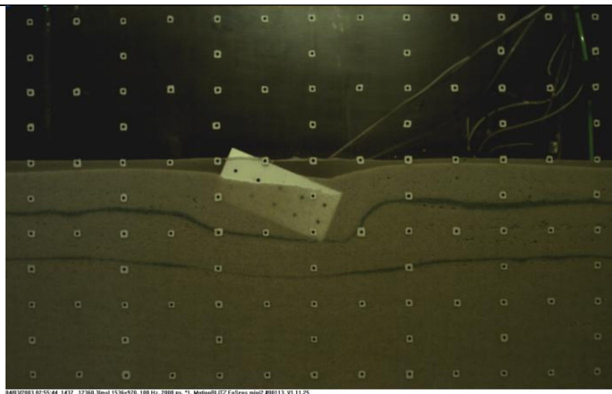
Figure 5.1.3 - Test 2 Earthquake 3	2mm Amplitude – 4.5 Hz

	
Figure 5.1.4 -Test 3 Earthquake 1	2mm Amplitude - 2.5 Hz

	
Figure 5.1.6 - Test 3 Earthquake 2	2mm Amplitude – 4 Hz

	
Figure 5.1.6 - Test 3 Earthquake 3	2mm Amplitude – 4 Hz

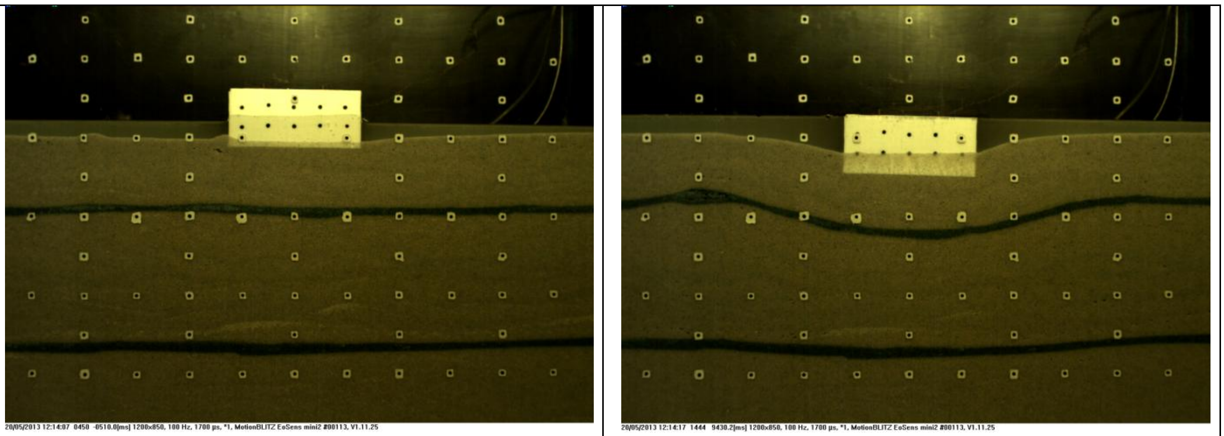

Figure 5.1.7 -Test 4 Earthquake 1	2mm Amplitude – 3.5 Hz

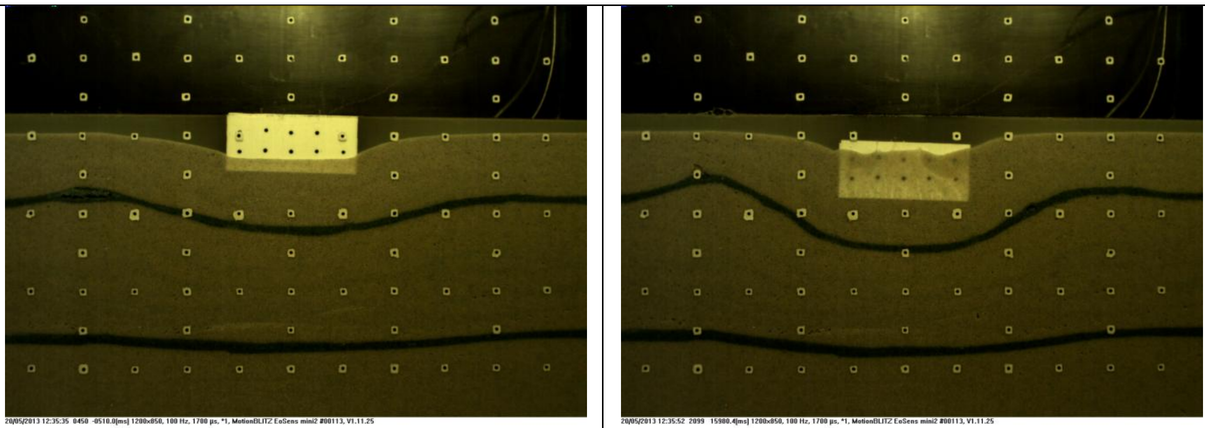

Figure 5.1.8 Test 4 Earthquake 2	2mm Amplitude 4 Hz

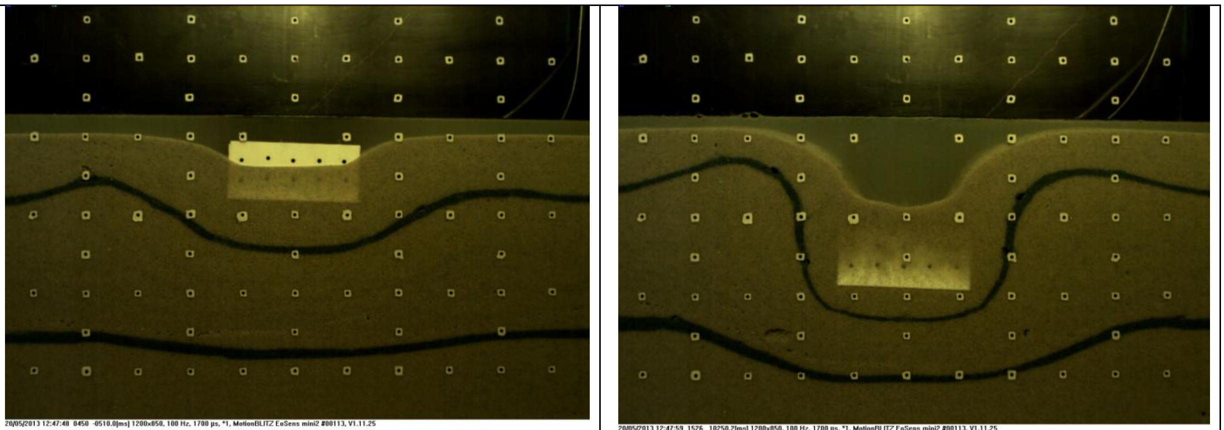

Figure 5.1.9 -Test 4 Earthquake 3	2mm Amplitude – 4.5 Hz

5.2 Visualisation of Foundation Failure

5.2.1 Summary

The PIV analysis has been utilised to investigate the movement of soil particles in order to 'visualise' the ground movements during foundation failure. This method has proved somewhat successful at tracking the soil patches during deformation; however, due to the magnitude of some of the soil movements between images, accumulated errors have been unavoidable, as the 'leapfrog' value must remain low (see section X). During testing, other phenomena were observed pertaining to the behaviour of liquefiable sands, and are discussed briefly in this section.

PIV Analysis - Test 1

As discussed in section 4, insufficient lighting and lack of texture was thought to have contributed to the poor quality of results from Test 1. Tests 2 through 4 adopted the procedure of adding dyed blue sand and using additional lighting, to increase the camera's perception of texture.

Half cycle Soil Movements

Given the driving force for failure in the experiments is the inertial load exerted by the structure, it is appropriate to view soil movements at peak acceleration. These accelerations will occur at the turning points of the structure's relative displacement from the shaking table box. A script, called guiqq, will calculate soil displacement vectors at four locations around the turning point in order to allow the development of the mechanism to be investigated.

5.2.2 High Aspect Ratio Tests

Low Acceleration Earthquakes

During low amplitude and frequency tests, there was little soil movement.

High Peak Acceleration Earthquakes

Test 2 Earthquakes 2 & 3 – Test 3 Earthquakes 2 & 3

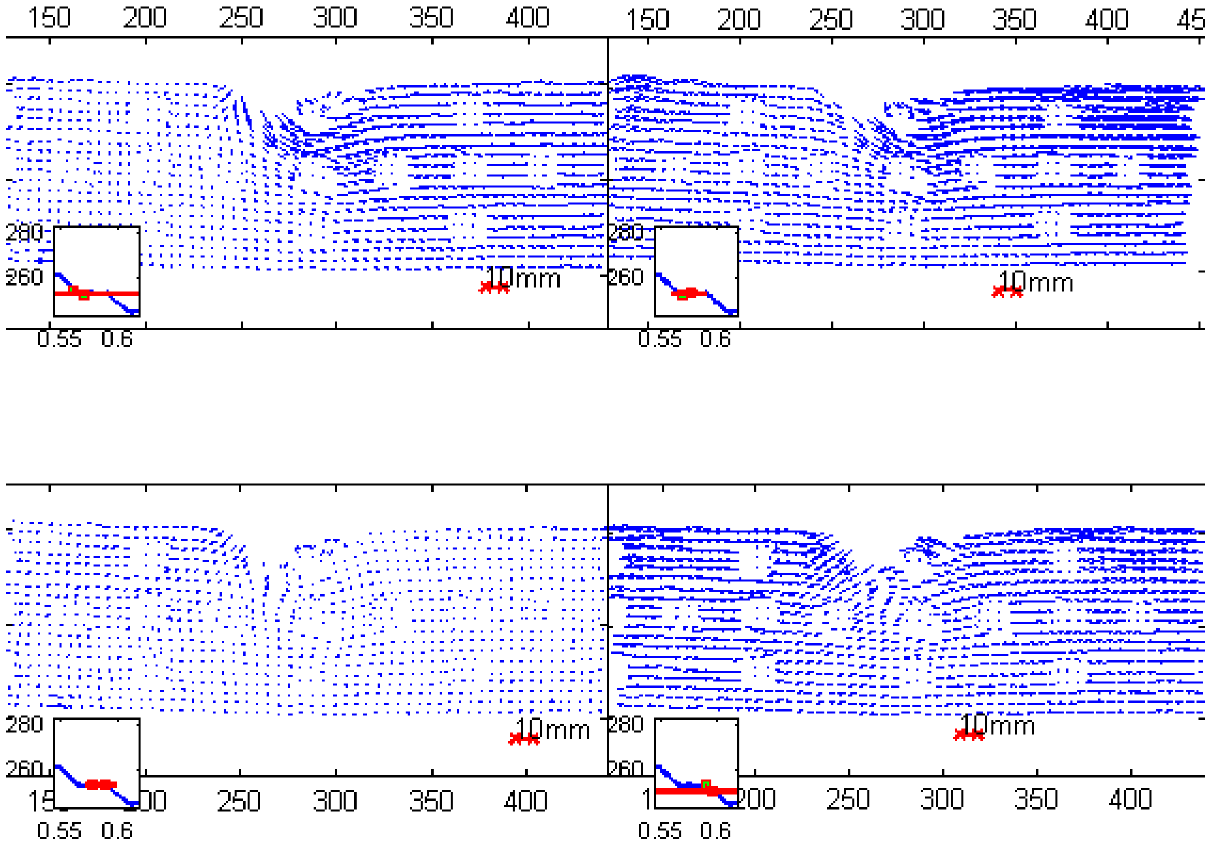

Fig. 5.2.1 - Soil displacement Vectors Test 2, Earthquake 3

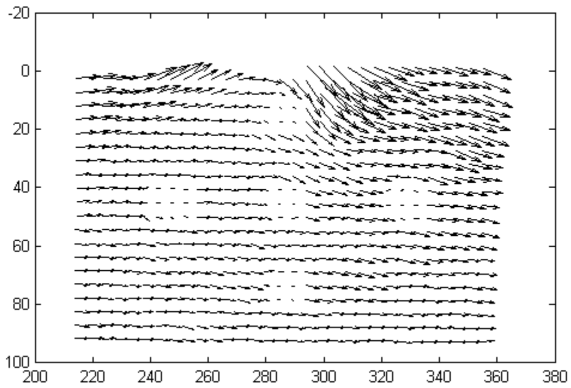

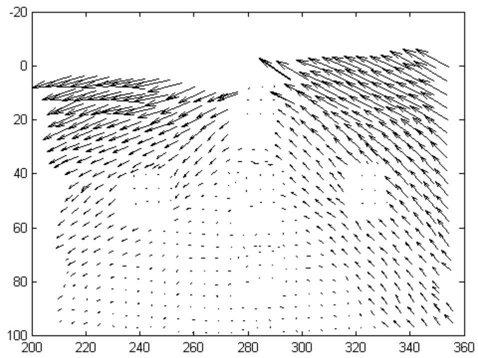

Fig. 5.2.2 a) - Test 3 Earthquake 3 - Initial mechanism

Fig. 5.2.2 -b) - Test 3 EQ 3 - Steady State Mechanism

The High acceleration (>0.3g) earthquakes in both cases the accelerations subjected to the high aspect ratio structures caused them to topple. Figures 5.2.1 a)-d) show the failure mechanism in Test 2 over a structural half cycle (water medium). This corresponds with the moment of uplift of the right hand corner of the structure, causing increased bearing on the remaining contact surface, leading to failure. A slip in fig. 5.2.1 a) mechanism can clearly be seen, which separates the left and right side of the figure, with a curved slip plane, similar to that obtained by Knappett (2006).

The final resting position of the foundation after earthquake three is similar to that of structures in the aftermath of the Niigata earthquake in 1964, whereby the rigid structure is (see Figure 1.4).

Earthquake 3 of Test 3 subjects the structure and soil model to accelerations of 0.13g. During the first few cycles of the earthquake (Figure 5.2.2), the structure settles more than in the water medium, meaning that it obtains greater support from the soil to resist toppling. At this point, a well defined failure mechanism similar to the drained case (figure 2.) is visible extending approximately 20mm below the footing. However, during subsequent cycles, the settlement mechanism becomes less well defined. During high acceleration phases of the cycle, large soil movements either side of the foundation have been observed but not directly underneath (Fig. 5.2.2 b)). The boundary between the three regions is clear, and is analogous to a rigid block mechanism. The abrupt change in soil displacement vectors is indicative of high strains. The uniform nature of the soil movements suggests that there is little resistance, and full liquefaction may have occurred in this region. It is likely that the cause of this divide is due to the increased stresses underneath the footing.

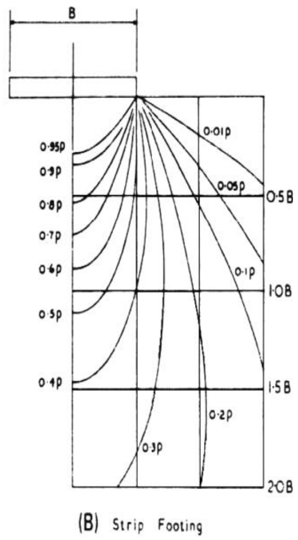

Fig. 5.2.3 - Theoretical Stress Distribution under a strip footing (after Boussinesq)

Figure 5.2.3 shows the theoretical stress distribution underneath a strip footing as presented by Boussinesq. This indicates that stresses from the foundation are not limited to its footprint. Subsequently, applying Terzaghi's Principle, a larger excess pore pressure would be required to cause a significant reduction in strength, as would be the case in liquefaction, given the greater total stress under and adjacent to the footing.

5.2.3 Low aspect ratio Structures

Test 4 – 2mm 3.5 Hz

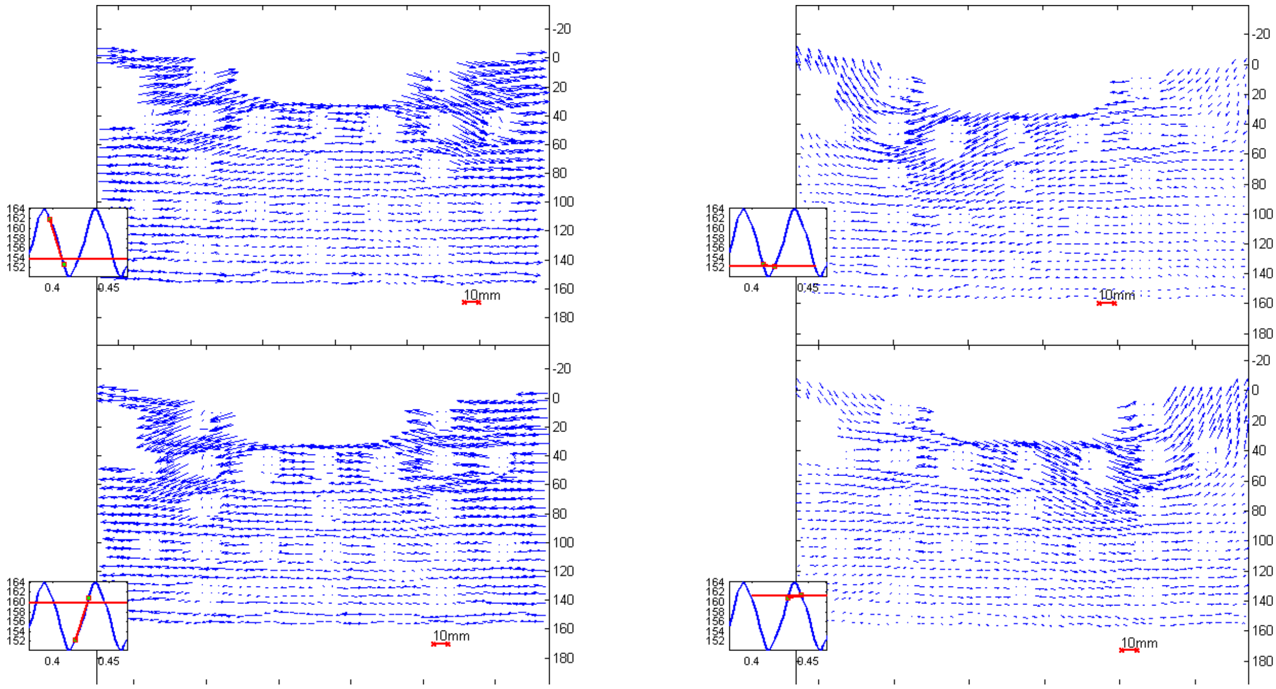

Fig. 5.2.4 (a-d) - Soil Movements for Test 4 EQ 2

Figure 5.2.4 shows the typical soil shearing pattern in the early stages of the earthquake motion. The relatively low moment applied to the structure during the earthquake accelerations has resulted in a shearing, or sliding mechanism, to a depth of 30mm couples with a punching baring mechanism at the embedded edges. Again, relative movements below the footing are small compared to either side. In addition, heave can be observed. In figure 5.2.4 d), a mechanism similar to the drained case is observable.

Free Field Settlements

As previously discussed, liquefied sand has a tendency to contract once pore pressures have dissipated. This leads to settlements in the free field, away from the influence of the foundation. Foundation Settlements therefore have been calculated relative to the free field settlements, as this will give more representative settlement behaviour. In addition, the relative settlement is a better indicator of the likely damage to services to a structure.

Some earthquake tests actually showed an overall heave effect, where the foundation settlement caused large heave action to occur (Figure 5.1.9)

5.2.5 Post Earthquake Settlements

It is well established that for drained analysis of soils, changes in voids ratio is related to the changing effective stress acting on the soil.. Given the excess pore pressures developed during earthquake tests, and applying Terzhagi's principle, it would therefore be expected that, as the pore pressures dissipated further subsidence of the foundation would occur. This is in keeping with observations of post earthquake settlements following real earthquake events (Ishihara 1973)

The PIV Analysis carried out to establish failure mechanisms during earthquake events has been extended to investigate post earthquake settlements. It has been found that no further settlement is recorded, between the end of ground movements and excess pore pressure dissipation.

Comparison of the post earthquake soil conditions with the Eurocode safety factor in Appendix A shows that even in the immediate aftermath of the earthquakes, with pore pressures at their highest, the safety factors remain well above 5 , i.e. the foundation will not fail or likely face any significant movements. This is because during the earthquake, the load is dynamic and inertial, placing much larger stresses on the soil. Statically, the total stresses and excess pore pressures are too low to have any real effect on movement the effective stress and therefore settlement. However, this could form the basis of further investigation. In addition, the stiff nature of the structure, which can be approximated as not having its own degrees of freedom, means inertial movements cease after the earthquake movement ends. Real structures, however, may continue to vibrate after ground movements have died away, leading to post earthquake settlements, as the soil remains excited by vibration.

5.2.6 Other Observed Phenomena

Unstable Slope Formation

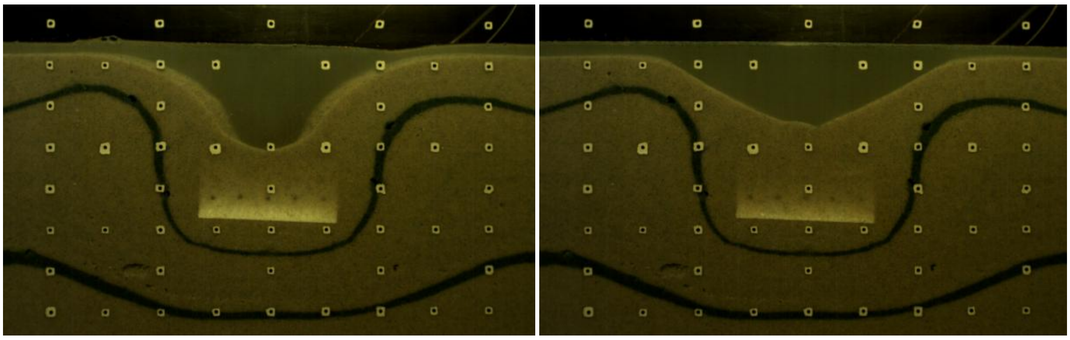

Fig. 5.2.5 (a & b) Unstable slope formation

Figure 5.2.5 (a) shows an image of the immediate aftermath of earthquake 3 during Test 4 (4mm amplitude, 4.0Hz driving frequency). It can be seen that the maximum slope angle is larger than 30 degrees (the critical friction angle of sand). Figure 5.2.5 (b) is an image taken a few minutes later, when the pore pressure readings had stabilised after the earthquake. This clearly shows the angle of the slope markedly reduced. This is likely to be the effect of negative pore pressures increasing in response to the particles dilating to form the curved slope, causing the sand particles to be forced together, creating a temporary increase in effective strength. When these pore pressures dissipate, the slope angle returns to the critical state. This is further evidence of the effect that pore fluid viscosity has on soil behaviour.

5.3 Pore Pressures Observations

5.3.1 Summary

Pore pressures in the soil model were measured under the footings at depths described in section 3.3. Table 5 displays the main findings of the pore pressure results. The rest of this section discusses the data and compares the responses for each test and earthquake.

Limitations

Low total confining stresses in the 1g shaking test limit the pore pressures that may be generated in the tests. As a result 300mbar PPTs are required to give sufficient resolution to such measurements. These are in limited supply, and as such only limited pore pressure data is available per test.

Pore Pressure Drift

The offset experienced by the pore pressure transducers after dissipation is simply the settlement of the instrument due to the soil movements. After dissipation, the new value is of pore pressure the additional hydrostatic pressure exerted by the pore fluid. This effect must be considered when discussing changes in excess pore pressures, as in later on in this section, where the concept is illustrated.

Comparison of High and Low Aspect Ratio Structures

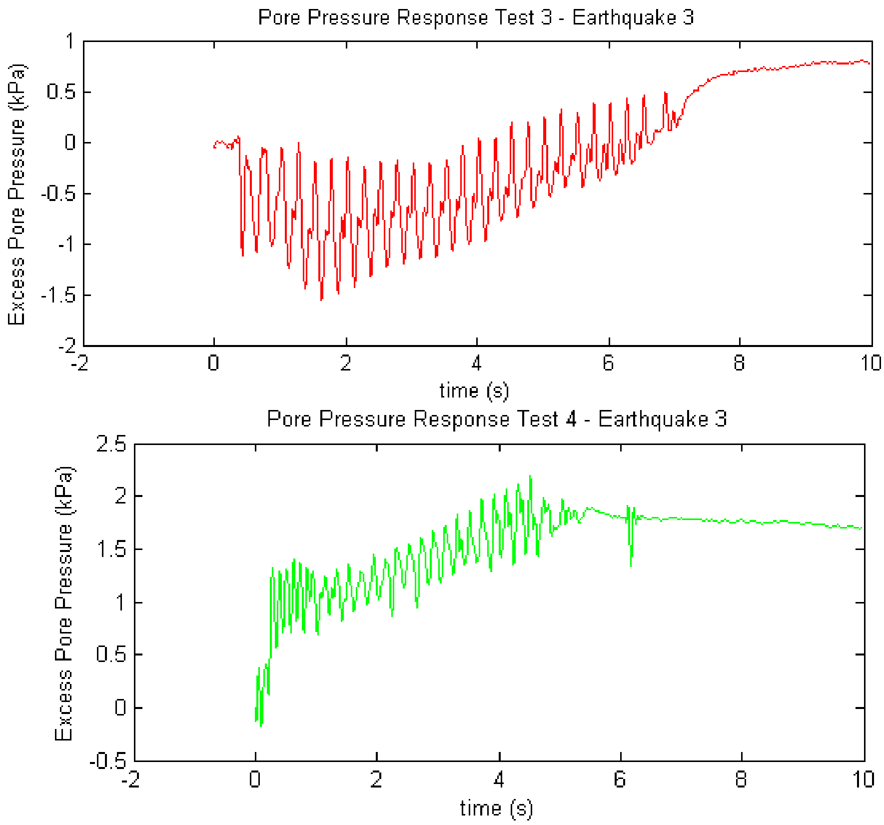

Fig.5.3.1 (a & b) High and low aspect ratio generated pore pressures

Figures 5.3.1 a & b show the pore pressure plots of two equivalent earthquakes from Tests 3 & 4 respectively (both Methylcellulose pore fluid). Peak driving accelerations were measured at the high aspect ratio model, applying a bearing stress of 7.7kPa on the soil exhibits the large negative excess pore pressure behaviour at the onset of the earthquake. As the earthquake progresses, the pore pressures increase cyclically, at a frequency double that of the driving frequency (8 Hz). The pore pressures continue to rise after the earthquake movements cease, before dissipating to the new hydrostatic level.

This is in contrast to the low aspect ratio model, which exerts a bearing pressure of 3.09kPa on the soil. At the beginning of the earthquake, the excess pore pressure rapidly increases to 0.9 kPa before steadily increasing during the test. At the end of the earthquake the excess pore pressure reaches a value of 1.6 before dissipating to 0.6kPa.

Peak to peak amplitudes have been calculated for both pore pressure responses, being 1.3 & 0.5kPa for Test 3 Earthquake 3 and Test 4 Earthquake 3 respectively. This ratio of 2.5 is consistent with the ratio of ground accelerations exerted by the shaking table. On first inspection of the pore pressure results for test 4 earthquake 3, the step change in pore pressures at the beginning of the cycle is similar to that of the excess pore pressure, i.e. the difference between pore pressures measured immediately following the earthquake and those measured at a steady value sometime in the future, after dissipation has occurred.

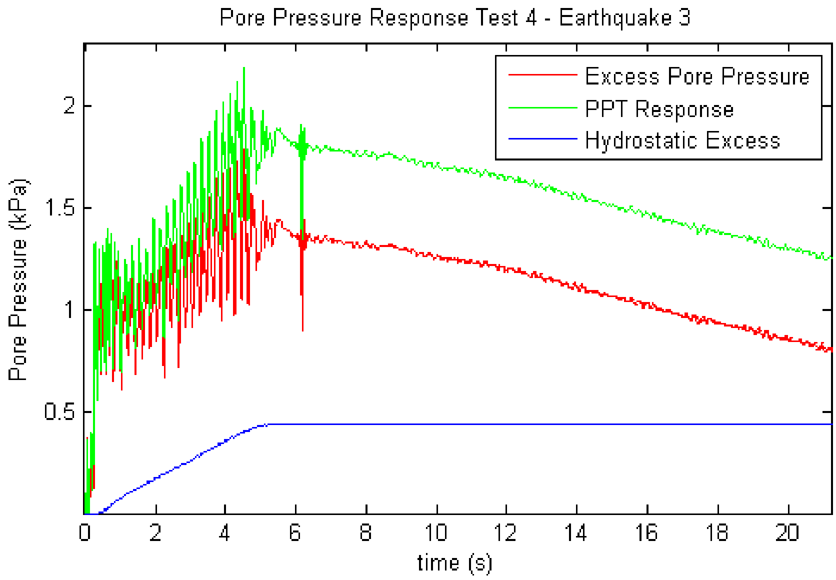

Fig. 5.3.2 – Test 4, Earthquake 3 original signal and an estimate of the corrected excess pore pressures

In order to establish the pure excess pore pressure behaviour of the earthquake, the hydrostatic component of the pressure due to settlement had to be estimated and subtracted from the reading. The settlement of the PPT was approximated by assuming plane deformations and measuring the settlement of the upper blue soil line using PIV. This settlement profile was superposed onto the signal to remove the hydrostatic component, resulting in the excess pore pressure behaviour in figure 5.3.2.

Shape of response

Figure 5.3.1 Shows the response of the Pore Pressure Transducer before, during and after the 2mm Amplitude, 4.0Hz earthquake. Before the earthquake begins the pore pressures are hydrostatic, consistent with their placement beneath the water table. It has been suggested that the additional noise of the signal before the earthquake may be partly due to the effect of the induction motor as it accelerates the flywheel.

Initially, the pore pressure transducer records a negative excess pore pressure, at the instant the shaking table begins to move. This negative excess pore pressure increases to a mean value of -0.8kPa after five cycles before increasing. The maximum excess pore pressure generated occurs at the end of the earthquake where an excess pore pressure of

0.8kPa is recorded. The excess pore pressure generated in the earthquake dissipates between 25 and 80 seconds, settling at a new value, 0.35kPa higher than previously.

Interpretation

Soil Behaviour under footing

The low aspect ratio tests exhibit the expected increase in pore pressure during the course of the earthquake event. As mentioned in Section 1, this is because in dry conditions loose sands tend to contract when subjected to cyclic shearing In high aspect ratio tests (tests 2 & 3), the PPTs were observed to record an initial drop in excess pore pressures. In the same logic as above with correlation between pore pressures and voids ratio, this suggests that initially the soil is dilating, causing the voids space occupied by the pore fluid to increase, resulting in a drop in pressure.

This may be related to the larger static bearing stress transmitted to the soil from the foundation, resulting in a higher confining stress in the region below the footing. This means that a greater monotonic, or static, stress profile is present in the soil before the earthquake begins.

Comparison of Pore Media

It is evident from table X that the viscosity of the pore fluid plays a key role in the behaviour of the soil model given the difference in time dissipation rates in water media (2s for Test 1) and Methylcellulose pore fluid (70s for Test 3: Earthquake 2). The figures also show that the

Table 5: Main Results from PPT Analysis	**Test 2**	**Test 3**	**Test 4**		
	EQ3	*EQ2*	*EQ1*	*EQ2*	*EQ3*
Minimum Neg. Pore Pressure	-0.2	-0.8	-0.2	0	0
Maximum Positive Pore Pressure	0.2	0.8	0.62	0.72	1.8
Hydrostatic drift (kPa)	-0.4	0.33	0.32	0.25	0.4
Dissipation Time (s)	2	70	75	80	95

maximum excess pres pressures generated in the soil occur once the forced shaking has finished, usually when the machine is winding down. These pore pressures continue to increase for longer in the methylcellulose pore fluid, reaching a higher maximum excess (see table 5). Comparison of the two high aspect ratio tests (Test 2 & 3) shows that the negative excess pore pressures experienced at the beginning of the earthquakes are markedly more distinct during the methylcellulose tests. This is due to the relative permeability of the sand to the two pore media. Pore pressures in the water dissipate before they have a chance to build up as the lower viscosity allows migration of pore pressures to occur with greater ease. This results in smaller excess pore pressures, which will affect the degree of liquefaction, as well as the amount of time the associated strength changes persist.

Scaling laws for 1g shaking table tests had suggested a pore viscosity of 30 cSt would be the most representative. It is unclear whether the differences between 1cSt and 10cSt pore fluid can be extrapolated to 30cSt, where they will be considered fully representative of the pressures found in reality.

Free Field vs. Structure Pore Pressure Response

Limited data is available relating to the differences between the free field pore pressures and the pore pressures under the structure. Figure 5.3.3 shows the pore pressure behaviour of the PPT's at position 1 (40mm below the surface directly underneath the foundation) and 2 (120mm below the surface in free field, 350mm from the centreline of the foundation).

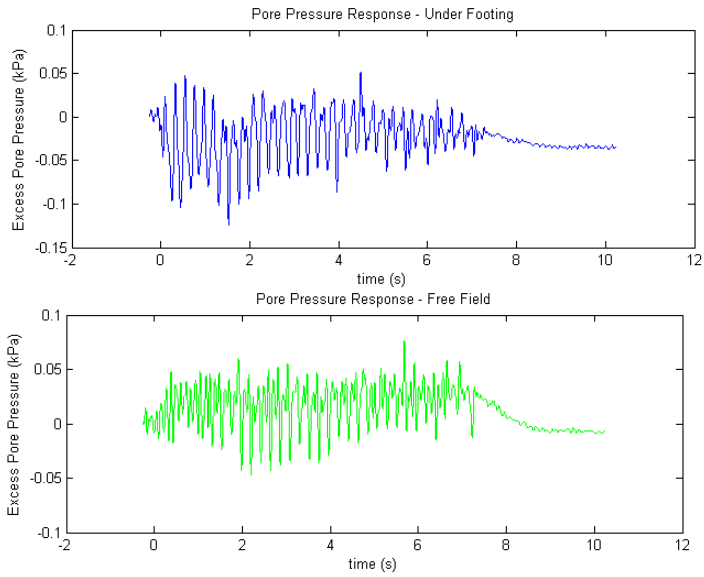

Fig 5.3.3 - Pore Pressures in Free field and under footing (Test 2 EQ3)

As described in Section 3, rapid dissipation of the excess pore pressure reduces the clarity of the figures, making behaviour less obvious. However, comparison of the two signals shows an initial reduction in pore pressure, corresponding to the dilative behaviour of the soil, under the structure. The free field pore pressure data shows no such reduction. This suggests that the soil stresses induced by the structure are the major cause of the behaviour. This may be related to the higher confining stress found under the footing than in the free field, which is acutely prevalent under the high aspect ratio (table 5).

5.4 Accelerometer Data

5.4.1 Summary

MEM accelerometers in the soil model and on the structure measure both horizontal and vertical accelerations during the earthquake tests. Analysis of the acceleration profile within the soil model will give an indication as to the depth of any failure mechanism, while comparison between soil and structural accelerations will identify the changing nature of the soil structure interaction. Phase information has been calculated

5.4.2High Aspect Ratio Structures

Low acceleration Earthquakes

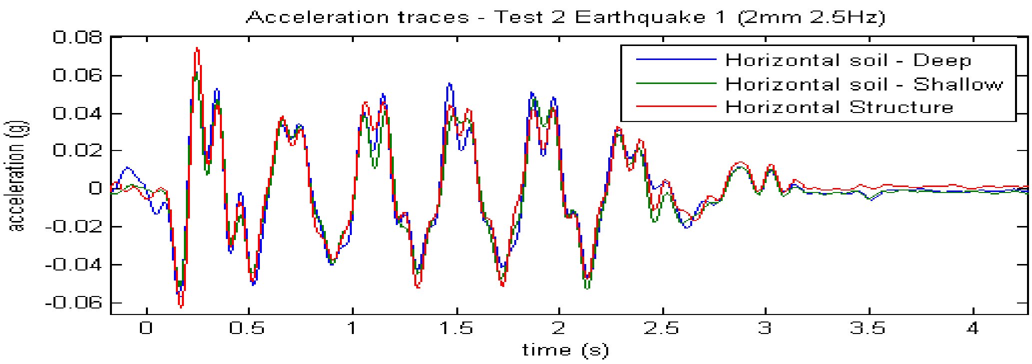

Figure 5.4.1 -Soil & Structural accelerations Test 2, Earthquake 1

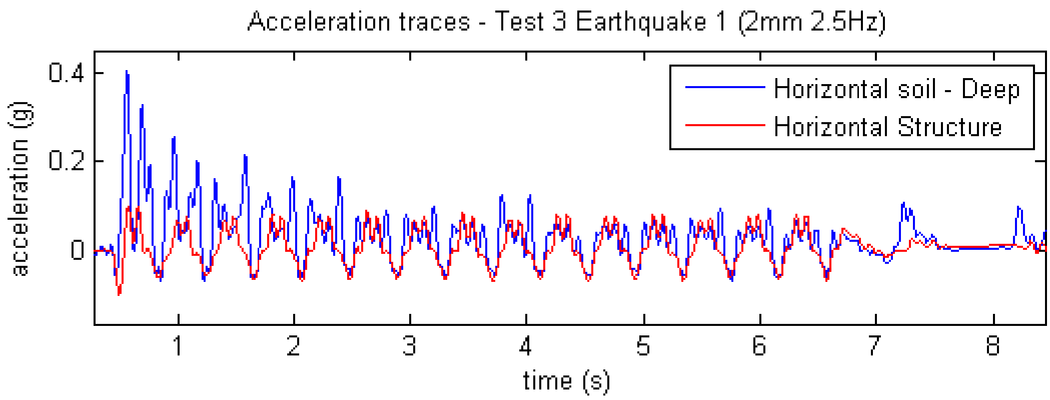

Figure 5.4.2 Soil & Structure Accelerations, Test 3, Earthquake 1

Figures 5.4.1 and 5.4.2 show the accelerations for 2mm, 2.5 Hz for tests two and three respectively. The structure and soil are in phase with one another, so it is likely that little settlements or relative movements will be observed during the PIV. There is some transience in the test 3 earthquake, which is a much higher amplitude than the driving accelerations (0.05g). Given that test 3 earthquake 1 had the high aspect ratio model embedded to a depth of 40mm, this may have had some effect on the deeper soil; however similar behaviour would be observed on the structural accelerometer.

High Acceleration Earthquakes

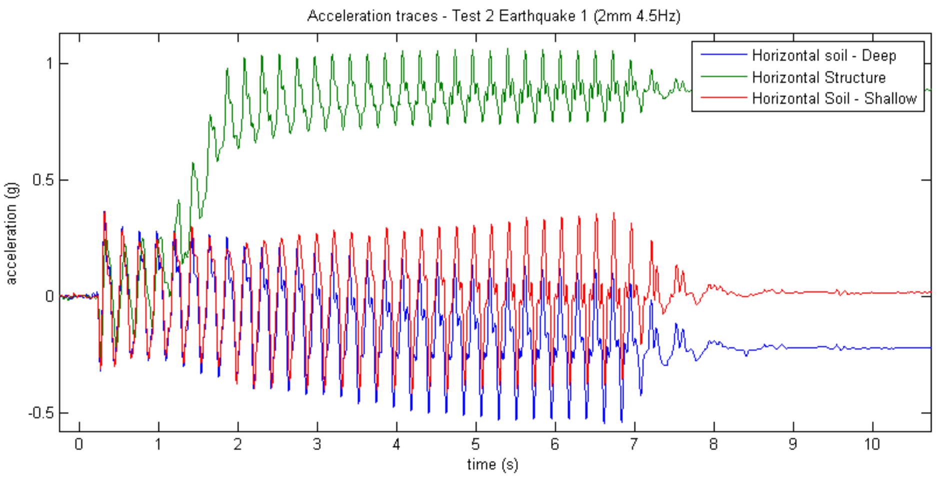

Fig. 5.4.3 – Soil and Structural Acceleration Traces; Test 2 Earthquake 3

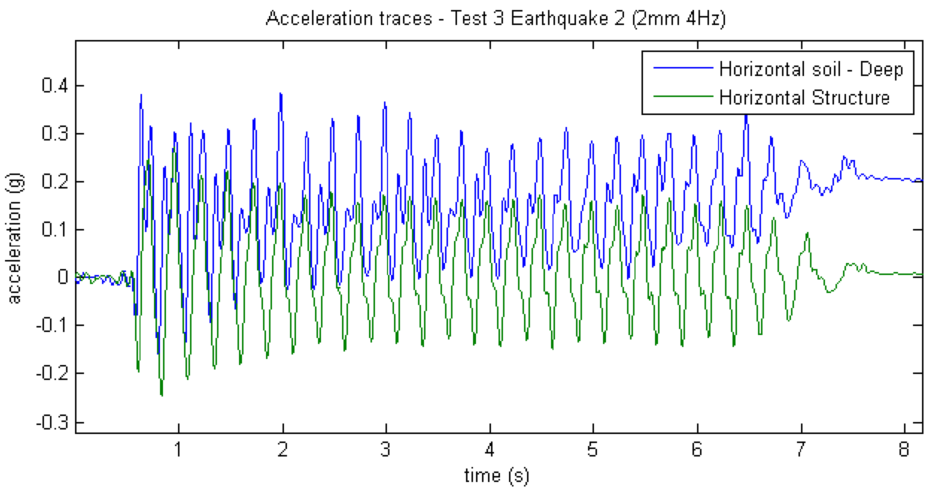

Fig. 5.4.4 - oil and Structural Accelerations; Test 3 Earthquake 2

Figures 5.4.3 and 5.4.4 show the acceleration traces of soil and structural MEMs detecting horizontal accelerations during 4.5 and 4 Hz earthquakes respectively, corresponding to peak accelerations of 0.16 and 0.14 g.

In figure 5.4.3, the increase in the structural acceleration trace corresponds to substantial rotation of the foundation as it fails during the earthquake. This also explains the reduction in cyclic amplitude; the accelerometer has rotated out of the plane of the driving acceleration (as discussed in section 3). The shallow and deep soil accelerometers remain in phase, but also display signs of drift. This may suggest non uniform soil movements. In particular between two and three seconds, both acceleration traces are drifting down together, before the shallow soil accelerometer returns back toward its zero point. This divergence coincides with the settlement of the structure in its toppled state (see Section 5.1).

Low Aspect Ratio Structures

Small acceleration earthquakes

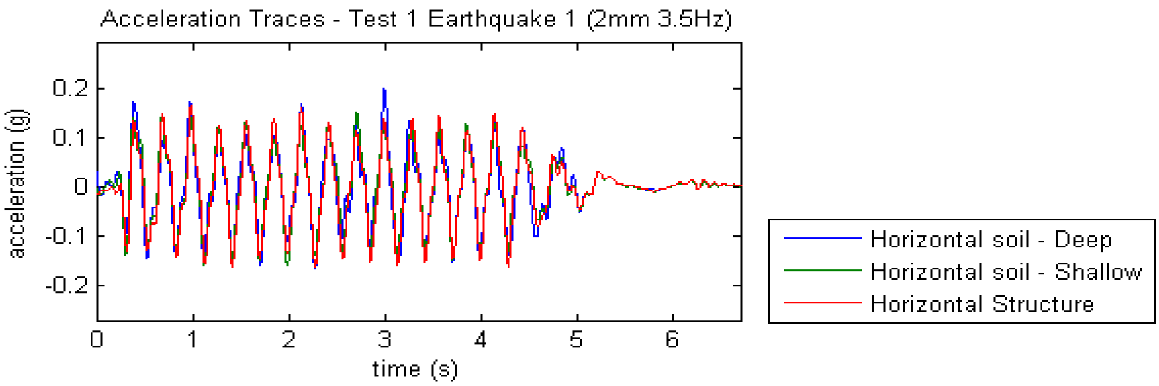

Fig. 5.4.5 Soil and Structural accelerations – Test 1: Earthquake 1

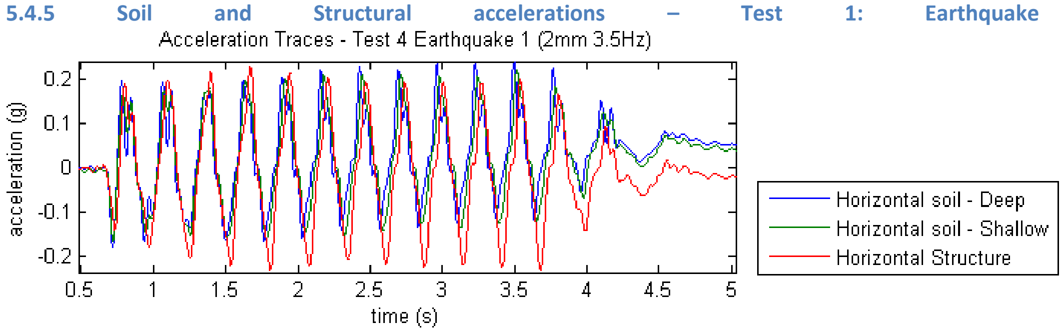

Figure 5.4.6 - Soil and Structural Accelerations : Test 4 Earthquake 4

Figures 5.4.5 & 5.4.6 show soil and structural accelerations of the low aspect ratio models in response to a 2mm amplitude, 3.5Hz earthquake. Test 1, with water pore fluid displays a similar response to the high aspect ratio model. The deep, shallow and structural accelerations are in phase and at the same amplitude, suggesting there is little relative sand movements under the structure.

Observing test four it is evident that the response of the structure is lagging that of the horizontal soil. This suggests that the soil foundation interface is no longer acting as a rigid boundary, and potentially slipping and deformations are occurring at the surface. Again offset acceleration traces are indicative of non-uniform soil movements

Large Acceleration Earthquakes

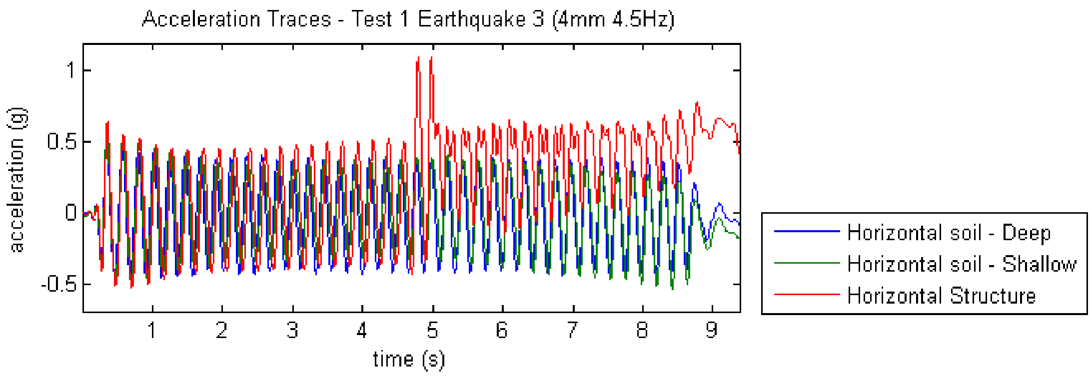

Fig. 5.5.7 - Soil and Structure Acceleration Traces - Test 1 EQ 3

Figure 5.5.7 shows the acceleration traces of the models in Test 1 in response to an earthquake of 4mm amplitude and 4.5Hz frequency, corresponding to a peak acceleration of 0.33g. In this the acceleration trace of the structure deviates from that of the soil MEMs, in terms of both phase and offset. Before 5 seconds the structural response can be seen deviating from that of the soil at a steady rate. suggesting progressive failure of the foundation.

6 Conclusions

The major aim of the project was to investigate the forms of foundation failures due to liquefaction events. Through experimentation and analysis, numerous behaviours associated with liquefaction events on 1g soil models have been identified and discussed.

- Methylcellulose & Water display different characteristics

  The behaviour of the soil was very much dependent on the viscosity of the pore fluid. Comparison of pore pressure data showed that for earthquakes of similar magnitudes, changes in pore pressure were different. This was compounded with PIV analysis which showed different types of mechanism for each pore fluid.
- Pore pressures affected by aspect ratio

  The aspect ratio and consequently bearing pressure had an effect on the types of mechanisms which were observed. Greater inertial moments on the footing lead to toppling collapse of the high aspect ratio structures. Pore pressures under the footings showed consistent differences between aspect ratios, with an initial drop in pore pressures for high aspect ratios, due to the influence of monotonic shearing in the soil increasing with bearing pressure. The superposition of static and dynamic shear patterns leads to the dilatent behaviour, as the sand is

- Soil Structure interaction changes over the course of the earthquake

  Changes in phase, magnitude and offset captured by the accelerometers gives an insight into the changing soil stiffness (and indeed strength) over the course of the event. PIV has showed that numerous failure mechanisms can be identified, over the course of a single earthquake.
- No additional settlements during pore pressure dissipation

  No detectable post earthquake settlements were observed throughout the tests. using the bearing capacity equation from Prandtl, with the empirical relationship estimate from Eurocode 7, it was found that, in post earthquake conditions, the static factors of safety were larger than 9. It is likely that being so far from bearing failure, the changes in effective stress will be too small to have any noticeable effect.

7 Future Work

This report documents the initial investigations into foundation behaviour during earthquake induced liquefaction. The project was qualitative in its approach, but will serve to inform and guide more in-depth research

Centrifuge Testing

Experiments undertaken in this experiment will be repeated using the centrifuge in the Schofield Centre. Testing in the centrifuge will allow a more realistic in situ stress profile, which will affect the drainage behaviour as well as the form of the mechanism. Phenomena such as negative excess pore pressure under high bearing foundations can be as pore pressure dropping

Further investigation into the causes and effects of documented post earthquake settlements could be undertaken. This could include soil structure interaction as well as response spectra, to investigate whether higher frequencies of shaking influence the behaviour of the bearing capacity of the sand.

Appendix A: Static Bearing Capacity using post earthquake soil conditions

$$V_{ult}/A = q_f = N_q\sigma'_{vo} + N_\gamma\gamma' {}^{B}/_{2}$$

Likely range of relative density is 0.4 -0.6

$$I_D = (e_{max} - e)/(e_{max} - e_{min})$$

e_{max}=1.067 e_{min}=0.555

Therefore

γ'_{40}=4.15 kN/m

γ'_{60}=4.96kN/m

High aspect ratio	Low aspect ratio
$\sigma'_{v0} = (7.7 + \gamma' z - \Delta u)$ kPa	$\sigma'_{v0} = (3.09 + \gamma' z - \Delta u)$ kPa

Ignoring self weight of sand term in σ'_{v0}

$$N_q = tan^2({}^{\pi}/_{4} + {}^{\varphi}/_{2})e^{\pi tan\varphi} \qquad (Prandtl, 1921)$$

$$N_\gamma = 2(N_q - 1)tan\varphi \quad (Eurocode\ 7)$$

Given φ = 30°

N_q=18.4 N_γ=20.09

Safety Factors for pre-dissipation post earthquake soil conditions

	Bearing Pressure (q)	Excess pore pressure measured Δu kPa	σ'_{v0} (kPa)	Ultimate capacity q_f (kPa)	Factor of Safety
Test 3: EQ2	7.7	0.8	6.9	128.62	16.7
Test 4:EQ1	3.09	0.62	2.47	50.43	16.32
Test 4: EQ2	3.09	0.72	2.37	48.59	15.72
Test 4: EQ3	3.09	1.8	1.29	27.9	9

8.2 Appendix B: Risk Assessment Retrospective

Initial Risk Assessment Submission

The initial risk assessment was carried out in conjunction with Dr. Gopal Madabhushi. Potential hazards regarding the project were identified and their risks assessed. Initially, these consisted of working with liquids and electrical equipment, heavy lifting as well as using some hazardous substances such as paints, silicones and glues. The potential risk of fine particulates from sand pouring was raised, which could have been considered a hazardous substance. However, upon further investigation it was decided that further action with regards a further risk assessment was not needed.

Risks encountered During Project & Mitigation

Heavy lifting

Large quantities of sand and liquids (water and methylcellulose solution) were required to be taken from the storage bins to the test rig. This was achieved with the use of pneumatic lifting equipment and cranes, to reduce the risk of injury during lifting.

Hazardous Substances

Hazardous substances included glues, flowable silicone as well as epoxy resins and metallic paints. Personal protection Equipment (PPE) including face masks and disposable gloves were used to reduce the exposure to such irritants.

Sand Pouring

Inhalation of fine sand particles had been identified as a key risk during the experimental setup. Precautions, including the use of a dust extractor and a face mask, were used during sand pours to reduce the risk of inhaling fine sand particles.

References

Paolucci, R. & Pecker, A. (1997) "Seismic bearing capacity of shallow strip foundations on dry soils." Soils and Foundations, 37(3), 95-105

Ishihara, K. (1993) Thirty Third Rankine Lecture "Liquefaction and flow failure during Earthquakes." Géotechnique Volume 43, Pages 349-417

Knappett, J.A., Haigh S.K., & Madabhushi S.P.G. (2006) "Mechanisms of Failure for shallow foundations under earthquake loading." Soil Dynamics and Earthquake Engineering 26(2006) 91-102

Douglas P Stewart et al. (1998) " Experience with the use of Methyl Cellulose as a Viscous Pore Fluid in Centrifuge Models"

Iai, S. (1989) "Similitude for shaking table tests on soil-structure-fluid model in 1g gravitational field." Soils and Foundations, 29(1), 105-118

White D.J, & Take W.A (2002) "GeoPIV: Particle Image Velocimetry (PIV) Software for use in geotechnical testing". CUED/D-SOILS/TR322

Acknowledgements

- Many thanks to my supervisor Dr. Gopal Madabhushi and Charlie Heron, for their guidance on theoretical and practical considerations throughout the year. To the other researchers and technicians at the Schofield Centre, for showing me the ropes and divulging their accumulated knowledge to minimise potential pitfalls.